Chemical Engineering Journal 143 (2008) 273–281

Contents lists available at ScienceDirect

Chemical Engineering Journal

journal homepage: www.elsevier.com/locate/cej

Catalytic decomposition of H_2S in a double-pipe packed bed membrane reactor: Numerical simulation studies

Francisco J. Trujillo, Kelfin M. Hardiman, Adesoji A. Adesina *

Reactor Engineering and Technology Group, School of Chemical Sciences and Engineering, University of New South Wales, NSW, 2052, Australia

ARTICLE INFO

Article history:
Received 5 December 2007
Received in revised form 16 February 2008
Accepted 18 February 2008

Keywords:
Membrane reactor
Co-current
Counter-current
Composite metallic membrane
H_2S catalytic decomposition

ABSTRACT

H_2 recovery from large quantities of toxic H_2S, the by-product of various minerals, coal and petroleum processing operations is an attractive proposition for efficient resource and energy utilization. This study has examined the analysis of a double-pipe membrane reactor internally packed with a Ru-Mo catalyst for the catalytic desulfurization of H_2S and H_2 generation. Due to the endothermic nature of the reaction, a non-isothermal model was employed. The effect of tube and shell-side residence times, sweep gas (argon) flow direction within the annular space between shell and inner membrane tube (relative to the H_2S feed) and the shell-to-tube side pressure ratio on H_2S conversion were investigated. The counter-current mode of reactor operation generally gave better H_2S conversions than the co-current mode (40–60%). Irrespective of shell-to-tube side pressure ratio, conversion in both modes of operation exceeded the thermodynamically-imposed ceiling by between two- and five-fold increase. The niobium membrane proposed was internally-coated with platinum to improve resistance to H_2S attack. The analysis showed that an optimum Pt thickness of about 1 μm is attainable although the possible formation of hairline cracks may necessitate the use of a higher coating. The model also accounted for the temperature-dependency of the membrane H_2 permeability in order to have a more realistic assessment of the reactor performance.

1. Introduction

H_2S is produced in large quantities during the processing of petroleum, coal and mineral ores. Along with H_2S from natural gas treatment, the annual global production is nearly three billon tones [1]. Although H_2S finds limited low-level use in the manufacture of sulfides, various organosulfur compounds and heavy water; due to its toxicity, H_2S must be removed or reduced to environmentally acceptable levels before disposal. Current technologies for the removal of H_2S from process off-gases depend on either the Claus process in which H_2S is burnt to release saleable sulfur and water, or absorption into caustic or amine solution such as the Selexol, Hot Carbonate process or the Alkazid process [2]. In the mineral processing industries, H_2S may also be removed via a number of thermochemical cycles involving metal oxide sulfidation followed by revivification as in the Dry-Box Process. While the net energy released from these routes may be used for low grade process heat requirements, it is evident that hydrogen utilized originally in the desulfurization process (either for crude petroleum, coal or mineral ores) is ultimately discarded as water. However, Raymont [3] has pointed out the beneficial economics of H_2 recovered from H_2S. Consequently, the splitting of H_2S into sulfur and valuable H_2, which can be recycled, has attracted investigation within the last three decades following Raymont's economic analysis. Catalytic desulfurization of H_2S has shown better promise in terms of yield and its kinetics and mechanism have been studied by different authors [4–6]. However, the reaction is highly endothermic (ΔH_{298} = 158 kJ mol^{-1}) and the equilibrium conversions are low (<10%) even at high temperatures (T > 1000 K) [7]. Since the reaction is equilibrium-limited, simultaneous separation of H_2 from the reaction will improve the process performance by shifting the equilibrium in favour of product formation [8]. It is in this respect that the catalytic packed bed membrane reactor becomes attractive.

Ceramic and composite metal membranes are commonly used for product separation in H_2-mediated reactions [8–10]. While ceramic membrane may be resistant to H_2S attack, they exhibit relatively poor selectivity towards H_2. However, metal membranes, for example, Pd, combine excellent mechanical strength with high H_2 selectivity and have therefore been used in many in-situ H_2-removal operations to achieve desired equilibrium shift [10–12]. For instance, Itoh [11] suggested that 100% conversion during cyclohexane dehydrogenation may be attained by using a palladium membrane reactor if the operating conditions are properly chosen. Even so, Pd and most metal membranes may be irreversibly attacked by H_2S leading to increased pore size and reduced permselectivity. Edlund and Pledger [13] have circumvented this constraint

* Corresponding author. Tel.: +61 2 93855268; fax: +61 2 93855966.
E-mail address: a.adesina@unsw.edu.au (A.A. Adesina).

1385-8947/$ – see front matter © 2008 Elsevier B.V. All rights reserved.
doi:10.1016/j.cej.2008.02.028

Nomenclature

$A = (2\pi rL)$ area of the membrane (m^2)
A_i internal tube area (m^2)
A_o external tube area (m^2)
C_H concentration of H^+ atoms on the membrane ($mol\ m^{-3}$)
$C^y_{H_2} = (C_{p^y_{H_2}} / C_{p^y_{mix_o}})$ dimensionless heat capacity of H_2 calculated at a particular point along the reactor y ("t" tube or "s" shell)
$C_{p^y_{H_2}}$ H_2 heat capacity ($J\ mol^{-1}\ K^{-1}$)
$C_{p^y_{mix_o}}$ heat capacity of the mixture at the inlet (y is "t" tube or "s" shell) ($J\ mol^{-1}\ K^{-1}$)
Da^t Damkohler number
Da^t_o initial Damkohler number (at the tube inlet)
D_s shell diameter (m)
D_{MA} diffusivity of H^+ atoms through the membrane ($m^2\ s^{-1}$)
D_t tube diameter (m)
E_a activation energy ($kJ\ mol^{-1}$)
F total molar flow rate of H_2 passing through the membrane ($mol\ s^{-1}$)
$F^s_{tot_o}$ initial total molar flux rate to the shell side ($mol\ s^{-1}$)
$F^t_{tot_o}$ initial total molar flow rate to the tube side ($mol\ s^{-1}$)
$\overline{F^y_{tot}} = \left(F^y_{tot}/F^y_{tot_o}\right)$ Dimensionless total flux on y, where y can be "t" for the tube or "s" for the shell.
$\overline{F^y_w} = \left(F^y_w/F^y_{tot_o}\right)$ dimensionless flux of the component w on y. The superscript y can be "t" for the tube or "s" for the shell. $w = H_2S, H_2$ or S_2.
h_f heat transfer coefficient from the furnace to the shell ($J\ m^{-2}\ s^{-1}\ K^{-1}$)
h_i internal tube heat transfer coefficient ($J\ m^{-2}\ s^{-1}\ K^{-1}$)
h_{io} $h_{io} = h_i(A_i/A_o)$
h_o external tube heat transfer coefficient ($J\ m^{-2}\ s^{-1}\ K^{-1}$)
h_{H_2} dimensionless H_2 flux through the membrane
$-\Delta H_{rxn}$ heat of reaction ($J\ mol^{-1}$)
$k_{H_2S}, k^o_{H_2S}$ reaction rate constants ($mol\ g\text{-}catalyst^{-1}\ s^{-1}\ kPa^{-0.5}$)
K equilibrium constant ($kPa^{-0.5}$)
K_s Sievert's constant ($mol\ m^{-3}\ kPa^{-0.5}$)
l longitudinal position on the reactor (m)
L total length of the reactor (m)
N_H flux of hydrogen atoms through the membrane ($mol\ m^{-2}\ s^{-1}$)
N_{H_2} flux of H_2 through the membrane ($mol\ m^{-2}\ s^{-1}$)
NHR dimensionless heat of reaction
P_{H_2} partial pressure of hydrogen (kPa)
P_{H_2S} partial pressure of H_2S (kPa)
P_{S_2} partial pressure of S_2 (kPa)
P^s_{tot} shell total pressure (kPa)
P^t_{tot} tube total pressure (kPa)
Q heat transfer rate from the shell to the tube ($J\ s^{-1}$)
r tube radius (m)
$\bar{r}$ average radius (m)
rts residence time on the shell (s)
rtt residence time on the tube (s)
R ideal gas universal constant $R = 8.31447\,e-3$ ($kJ\ mol^{-1}\ K^{-1}$)
R_f ratio of the feed total molar flow rate through the tube $F^t_{tot_o}$ to the feed total molar flow rate through the shell $F^s_{tot_o}$. $R_f = \left(F^t_{tot_o}/F^s_{tot_o}\right)$
R_h $R_h = \left(h_{io}/h_i\right)$
R_p ratio between the total pressure of the shell P^s_{tot} and the total pressure of the tube P^t_{tot}. $Rp = \left(P^s_{tot}/P^t_{tot}\right)$
$St^t, St^s, St_s{}^t$ Stanton numbers
T^f furnace temperature (K)
T^s shell temperature (K)
T^s_o initial shell temperature (inlet) (K)
T^t tube temperature (K)
T^t_o initial tube temperature (inlet) (K)
Tu dimensionless number that represents the ratio of the hydrogen permeation rate to the tube feed rate.
T_w wall temperature (K)
U_{H_2} permeation coefficient ($mol\ s^{-1}\ kPa^{-0.5}$)
U^{tg} overall heat transfer coefficient between the tube and shell
V volume of the tube reactor (m^3)
V^s volume of the annular shell (m^3)
y^y_w molar composition of the component w on y, where $w = H_2S, H_2, S_2$ or Ar, and y = "t" for tube or "s" for shell
$z = \frac{l}{L}$ dimensionless longitude of the tube. $z = (l/L)$

Greek letters
$-\gamma_{H_2S}$ kinetic rate of reaction ($mol\ m^3\ s^{-1}$)
$\left(-\gamma_{H_2S}\right)_{th}$ thermal decomposition kinetic rate ($mol\ m^3\ s^{-1}$)
δ membrane thickness (m)
ε_b catalyst bed void fraction
ρ_{bed} catalyst bed density ($g\text{-}catalyst\ m^{-3}$)
ρ_{MA} membrane permeability ($mol\ m^{-1}\ s^{-1}\ kPa^{-0.5}$)
ρ^s_{mol} molar density of the fluid on the shell ($mol\ m^{-3}$)
ρ^t_{mol} molar density of the fluid on the tube ($mol\ m^{-3}$)
$\Phi^f = \left(T^f/T^t_o\right)$ dimensionless temperature of the furnace
$\Phi^s = \left(T^s/T^t_o\right)$ dimensionless temperature of the shell
$\Phi^t = \left(T^t/T^t_o\right)$ dimensionless temperature of the tube

Subscripts
Nb niobium
o initial (at the inlet)
Pt platinum
tot total
tot_o total at the inlet

Superscripts
s shell
t tube

using a vanadium membrane coated with Pt (strongly resistant to H_2S attack) on the reactive (interior) side where the corrosive H_2S is produced. Such a composite metal membrane was reportedly thermally stable up to 973 K. In fact, the permselectivity of several metallic membranes as function of temperature has been studied by Buxbaum and Kinney [14]. Their data suggested the superiority of Nb over many other transition metals as membrane when high H_2 permselectivity is required. Consequently, a Pt-coated Nb membrane has been employed in the present work.

Fukuda et al. [15] found that the molybdenum disulfide MoS_2 is an effective catalyst for the decomposition of H_2S over the range 773–1073 K. They reported more than 95% conversion of the H_2S

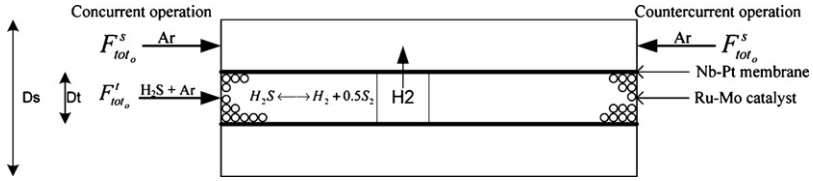

Fig. 1. Membrane catalytic reactor operated in either co-current or counter-current mode.

into hydrogen and sulfur by intermittent separation of hydrogen from the reaction gas mixture in a Vycor glass packed reactor. Kaloidas and Papayannakos [16] have also derived a Langmuir-Hinshelwood kinetic model for hydrogen sulfide decomposition on MoS_2. Adesina and co-workers [5,17,18] also studied the hydrogen sulfide decomposition on CoS-MoS_2 [18] and Ru-Mo sulfide [17] catalysts finding higher activities than with MoS_2. The best performance was achieved with the Ru-Mo sulfide catalyst which exhibited an activity about four times higher than other supported catalysts previously reported.

Analysis of shell and tube membrane reactors in the literature has been mostly focused on co-current flow (between the feed and sweep gas) operation [7–9,19]. However, the possible advantages – for example, improved heat transfer efficiency – that may be offered by the counter-current operation as exhibited by double-pipe heat exchangers are well known [20]. Zaman and Chakma [19] carried out the modeling of H_2S thermal decomposition in a co-current membrane reactor and concluded that for high sweep gas flow rates, high conversions may be achieved by using high temperatures, thin-wall membranes and a reactor configuration with high surface to volume ratio and a high reactor residence time. At low sweep gas rates, conversions approached limiting values depending of the other process conditions. In a previous study, Chan et al. [8] also showed that the performance of a co-current H_2S catalytic membrane reactor improved the H_2 yield beyond the equilibrium values. Significantly, that investigation neither admitted the temperature-dependency of the membrane permeability nor variation in the Pt layer thickness in the reactor analysis. Indeed, as discussed later, the treatment of the counter-current mode of operation is a nonlinear boundary-value problem rather than an initial-value problem and hence, distinctly more involving from a mathematical analysis standpoint. Thus, the objective of the present work is to develop a robust model that permits the realization of these attributes as well as the contributions of homogeneous decomposition to the overall reaction rate in order to obtain a realistic comparison of the performance between co- and counter-current operation of the double-pipe packed bed catalytic membrane reactor.

2. Model development

A schematic diagram of the shell and tube membrane reactor is shown in Fig. 1. The feed to inner tube packed with Ru-Mo sulfide catalyst is an H_2S/argon mixture. The sweep gas through the annulus was pure argon. Table 1 shows the reactor properties.

2.1. Hydrogen transport through the membrane

Hydrogen transport through metals has been studied extensively [14]. It is known that hydrogen molecules (H_2) dissociate into hydrogen atoms to diffuse through metals. For the geometry shown in Fig. 2, the flux of hydrogen atoms may be described by Fick's law as:

$$N_{H^+} = -D_{MA}\frac{\partial C_H}{\partial r} \quad (1)$$

Table 1
Membrane reactor characteristics and operating conditions

Parameter	Values
Length of the reactor L	0.6 m
Diameter of the tube D_t	9.017×10^{-3} m
Diameter of the shell D_s	1.96×10^{-2} m
Thickness of niobium membrane	$1. \times 10^{-3}$ m
Thickness of platinum film	2.5×10^{-5} m
Total operating pressure P^t_{tot}	101.325 kPa
Tube inlet temperature = shell inlet temperature = furnace temperature, $T^t_o = T^s_o = T^f$	973.15 K
Tube inlet composition	20% H_2S, 80% argon
Shell inlet composition	100% Argon

where N_H is the flux of H, D_{MA} is the diffusivity of hydrogen atoms through the membrane, r is the radius and C_H is the concentration of hydrogen in the metal, which is in equilibrium with the partial pressure of hydrogen in the fluid side according to the Sievert's law:

$$C_H = K_s {P_{H_2}}^{1/2} \quad (2)$$

K_s is the Sievert constant and P_{H_2} is the partial pressure of hydrogen. Thus, the flux of H atoms through the membrane can be expressed as a function of the hydrogen partial pressure by combining Eqs. (1) and (2):

$$N_H = -D_{MA}K_s \frac{\partial {P_{H_2}}^{1/2}}{\partial r} \quad (3)$$

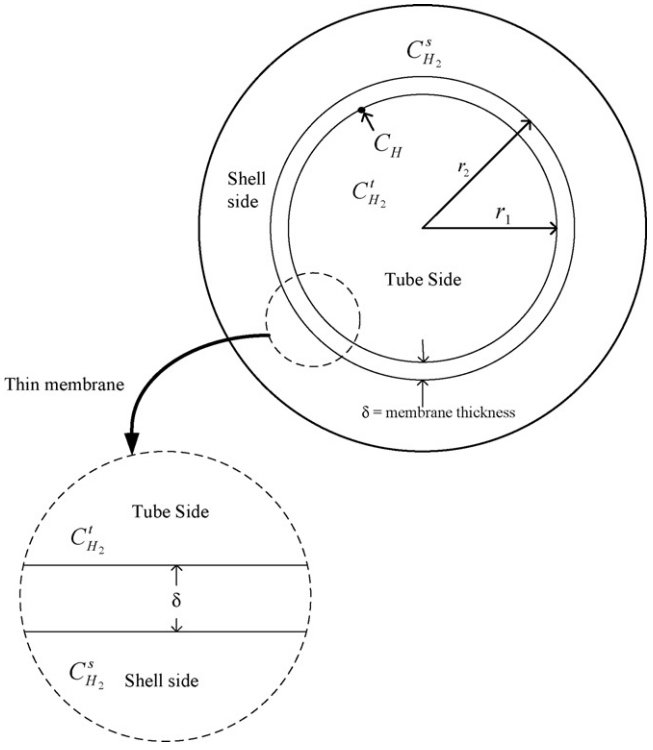

Fig. 2. Cross sectional view of the tube-and-shell membrane reactor.

The flux of hydrogen molecules (H_2) is half the flux of hydrogen atoms:

$$N_{H_2} = -\rho_{MA}\frac{\partial P_{H_2}^{1/2}}{\partial r} \tag{4}$$

where the term $\rho_{MA} = D_{MA}K_s/2$ is the permeability of the material [14]. Thus, the material balance across the curved surface area for the inner tubular reactor is given by:

$$F = -\rho_{MA}(2\pi rL)\frac{\partial P_{H_2}^{1/2}}{\partial r} \tag{5}$$

Integrating over the tube thickness yields:

$$F\int_{r_1}^{r_2}\frac{\partial r}{r} = -\rho_{MA}(2\pi L)\int_{P_{H_2}^t}^{P_{H_2}^s}\partial P_{H_2}^{1/2} \tag{6}$$

Hence, the H_2 flux through the membrane can be expressed as:

$$N_{H_2} = \frac{F}{A} = \frac{F}{(2\pi\bar{r}L)} = \frac{\rho_{MA}}{\bar{r}\ln(r_2/r_1)}((P_{H_2}^t)^{1/2} - (P_{H_2}^s)^{1/2}) = U_{H_2}(\Delta P_{H_2}^{1/2}) \tag{7}$$

where the permeation coefficient U_{H_2} is defined as:

$$U_{H_2} = \frac{\rho_{MA}}{\bar{r}\ \ln(r_2/r_1)} \tag{8}$$

In the case of multiple metal layers, the total transport resistance may be obtained from:

$$\frac{1}{U_{H_2}} = \sum_i \frac{\bar{r}_i\ \ln(r_{ext_i}/r_{int_i})}{\rho_{MA_i}} \tag{9}$$

If the membrane thickness is very small compared with the radius of the reactor ($r_2 \approx r_1$) the analysis simplifies to:

$$N_{H_2} = \frac{F}{A} = \frac{\rho_{MA}}{\delta}\left((P_{H_2}^t)^{1/2} - (P_{H_2}^s)^{1/2}\right) = U_{H_2}(\Delta P_{H_2}^{1/2}) \tag{10}$$

where A and δ are the area and thickness of the membrane respectively. The permeation coefficient is defined as:

$$U_{H_2} = \frac{\rho_{MA}}{\delta} \tag{11}$$

and for a multilayer metal composite, U_{H_2} may be obtained from:

$$\frac{1}{U_{H_2}} = \sum_i \frac{\delta_i}{\rho_{MA_i}} \tag{12}$$

Niobium was chosen as the membrane material due to its high permeability to hydrogen [14]. The tube-side of the membrane is coated with a layer of platinum to ensure the resistance of the membrane to the H_2S attack. The platinum layer must, however, be thin because of its low H_2 permeability. Buxbaum and Kinney [14] have provided plots of the H_2 permeability for several metals as a function of temperature. From these data the temperature-dependent permeability for Pt and Nb were obtained as:

$$\rho_{MA_{Pt}} = \frac{-3.6893\times10^{-6}}{T} + 5.281\times10^{-9}$$
$$\rho_{MA_{Nb}} = \frac{4.3122\times10^{-2}}{T} - 3.0484\times10^{-5} \tag{13}$$

where $\rho_{MA_{Pt}}$ and $\rho_{MA_{Nb}}$ are the H_2 permeability (mol m^{-1} s^{-1} kPa$^{-0.5}$) for Pt and Nb respectively.

2.2. Kinetic model for catalytic H_2S decomposition

The catalytic decomposition of H_2S over alumina supported Ru-Mo sulfide over the range 863–973 K has been experimentally investigated in our laboratory by Gwaunza and Adesina [17]. The data from that study were used to evaluate the kinetic parameters of the reversible reaction rate model employed in this paper. The reversible H_2S decomposition written;

$$H_2S \rightleftharpoons H_2 + \frac{1}{2}S_2 \tag{14}$$

may be described by:

$$-\gamma_{H_2S_{catalytic}} = k_{H_2S}(P_{H_2S} - \frac{1}{K_{eq}}P_{H_2}P_{S_2}^{1/2})\rho_{bed} \tag{15}$$

where,

$$k_{H_2S} = k_{H_2S}^o e^{-E_a/RT} \tag{16}$$

and K is the equilibrium constant. A fit of the experimental data at four different temperatures between 863 and 973 K gave, $k_{H_2S}^o = 3.8505\times10^{-2}$ mol g-catalyst^{-1} s^{-1} kPa^{-1}, E_a = 87.22 kJ mol^{-1}, ρ_{bed} is the catalyst bed density and R is the gas constant (=8.314 J mol^{-1} K^{-1}) where K_{eq} is given by [6];

$$K_{eq} = 3782e^{-10871/T}\ \text{kPa}^{1/2} \tag{17}$$

Fig. 3 shows good agreement between the empirical data and the kinetic model. Homogeneous thermal gas phase decomposition of H_2S is significant at temperatures greater than 973 K as demonstrated by the data of Kaloidas and Papayannakos [4]. They have proposed an expression for this non-catalytic rate as:

$$-\gamma_{H_2S_{thermolysis}} = k_{hom}\left(P_{H_2S} - \frac{1}{K_{eq}}P_{H_2}P_{S_2}^{1/2}\right) \tag{18}$$

where,

$$k_{hom} = 7.740e^{-195811.2/RT}\ \text{mol cm}^{-3}\ \text{s}^{-1}\ \text{kPa}^{-1} \tag{19}$$

Fig. 4 illustrates the comparison between the catalytic and thermal decomposition rates for a feed with 20% H_2S/argon as a function of temperature when the total reactor pressure is 101.3 kPa. In order to obtain a representative performance of the double-pipe membrane packed bed reactor, a hybrid rate equation which accounts for the contribution of the direct gas phase thermolysis was employed. Thus, the rate equation used in the reactor modeling below is;

$$(-\gamma_{H_2S}) = (-\gamma_{H_2S_{catalytic}}) + (-\gamma_{H_2S_{thermolysis}})\varepsilon_{bed} \tag{20}$$

where ε_{bed} is the bed voidage.

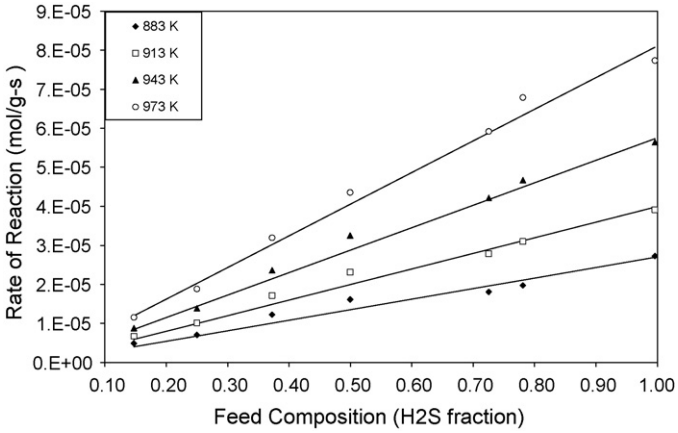

Fig. 3. H_2S decomposition rate as a function of feed composition for alumina supported Ru-Mo sulfide catalyst. (Experimental data obtained by Gwaunza and Adesina [17]).

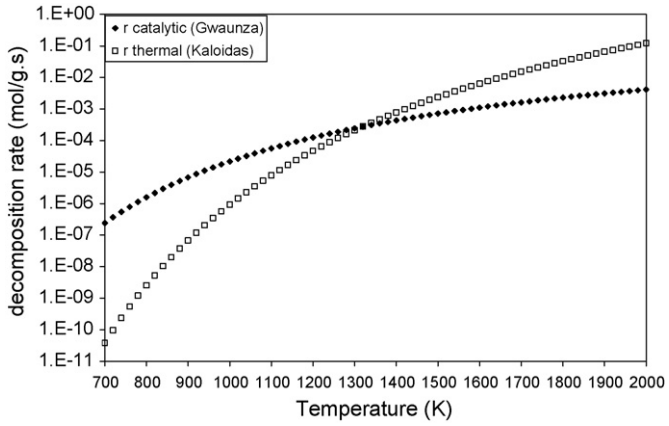

Fig. 4. Catalytic and thermal decomposition rate models for a feed with 20% H_2S.

2.3. Membrane reactor model equations

In order to simplify the analysis of the membrane reactor, it is assumed that:

1. Plug flow conditions exist in both the shell and tube side.
2. Negligible axial pressure drop prevails in both packed bed and annular space.
3. H_2 permeation through the membrane follows Eq. (10).
4. Neither H_2S nor S_2 molecules permeate through the membrane, i.e. 100% H_2 permselectivity.
5. The Pt-coated Nb membrane is catalytically inactive.
6. Reactant and sweep gas can flow co- or counter-current.
7. The reactor is operated non-isothermally ($\Delta H_{298} = 158\ \mathrm{kJ\ mol^{-1}}$) [20].

Based on these assumptions the steady-state mass and energy balance equations for the membrane reactor are:

Tube-side:

H_2S balance

$$\frac{\mathrm{d}(\overline{F^{\mathrm{t}}_{\mathrm{H_2S}}})}{\mathrm{d}z} = -Da^{\mathrm{t}} \tag{21a}$$

where Da^{t} is the tube-side Damkholer number.

H_2 balance

$$\frac{\mathrm{d}(\overline{F^{\mathrm{t}}_{\mathrm{H_2}}})}{\mathrm{d}z} = Da^{\mathrm{t}} - \mathrm{Tu}((y^{\mathrm{t}}_{\mathrm{H_2}})^{\frac{1}{2}} - (R_{\mathrm{p}} y^{\mathrm{s}}_{\mathrm{H_2}})^{\frac{1}{2}}) \tag{21b}$$

Tu is the ratio of the H_2 permeation rate through the tube and molar feed rate to the tube and R_{p} is the total pressure ratio between the shell and tube sides.

S_2 balance

From the reaction stoichiometry, the tube-side S_2 flux may be estimated from:

$$\overline{F^{\mathrm{t}}_{\mathrm{S_2}}} = \frac{\overline{F^{\mathrm{t}}_{\mathrm{H_2S}}} - \overline{F^{\mathrm{t}}_{\mathrm{H_2S}}}}{2} \tag{21c}$$

Shell-side:

H_2 balance

$$\frac{\mathrm{d}(\overline{F^{\mathrm{s}}_{\mathrm{H_2}}})}{\mathrm{d}z} = \pm[-\mathrm{Tu}R_{\mathrm{f}}((y^{\mathrm{t}}_{\mathrm{H_2}})^{1/2} - (R_{\mathrm{p}} y^{\mathrm{s}}_{\mathrm{H_2}})^{1/2})] \tag{21d}$$

where R_{f} is the ratio of the total feed molar flow rate through the tube-side to that through the shell-side.

Tube-side energy balance:

$$\frac{\mathrm{d}(\overline{F^{\mathrm{t}}_{\mathrm{tot}}}\overline{C_{p^{\mathrm{t}}_{\mathrm{mix}}}}\overline{\Phi^{\mathrm{t}}})}{\mathrm{d}z} = Da^{\mathrm{t}} \cdot \mathrm{NHR} - J_{\mathrm{H_2}} C^{\mathrm{t}}_{\mathrm{H_2}} \Phi^{\mathrm{t}} - St^{\mathrm{t}}(\Phi^{\mathrm{t}} - \Phi^{\mathrm{s}}) \tag{21e}$$

where NHR is the dimensionless heat of reaction, $J_{\mathrm{H_2}}$ is the dimensionless H_2 flux across the membrane while Φ's are the dimensionless temperatures as defined in the Nomenclature section.

Shell-side energy balance:

$$\frac{\mathrm{d}(\overline{F^{\mathrm{s}}_{\mathrm{tot}}}\overline{C_{p^{\mathrm{s}}_{\mathrm{mix}}}}\overline{\Phi^{\mathrm{s}}})}{\mathrm{d}z} = \pm\left\{-J_{\mathrm{H2}} R_{\mathrm{f}} C^{\mathrm{s}}_{\mathrm{H_2}} \Phi^{\mathrm{t}} - St^{\mathrm{s}}(\Phi^{\mathrm{f}} - \Phi^{\mathrm{s}}) - St^{\mathrm{t}}_{\mathrm{s}}(\Phi^{\mathrm{t}} - \Phi^{\mathrm{s}})\right\} \tag{21f}$$

where the signs (+) and (−) in Eqs. (21d) and (21f) apply to counter- and co-current operations respectively. The dimensionless component molar rates are defined as:

$$\overline{F^{y}_{\mathrm{w}}} = \frac{F^{y}_{\mathrm{w}}}{F^{y}_{\mathrm{tot_o}}} \tag{22}$$

where the subscript "w" indicates the component (w = H_2S, H_2 or S_2). The superscript "y" stands for tube (t) or shell (s), and $F^{y}_{\mathrm{tot_o}}$ represents the total initial flow rate to "y"-side (tube or shell). The model takes in account the total flow rate (F^{y}_{tot}) through the tube and shell changes inside the reactor with position as a consequence of the H_2 permeation through the membrane. Hence, the dimensionless total molar flow rate ($\overline{F^{y}_{\mathrm{tot}}}$) is defined as:

$$\overline{F^{y}_{\mathrm{tot}}} = \frac{F^{y}_{\mathrm{tot}}}{F^{y}_{\mathrm{tot_o}}} \tag{23}$$

where $F^{y}_{\mathrm{tot_o}}$ is the feed molar flow rate to the y-side.

The component balance Eqs. (21a–d) are clearly dependent on the dimensionless numbers, Damkholer (Da^{t}) and Tu which are defined as:

$$Da^{\mathrm{t}} = \frac{-\gamma_{\mathrm{H_2S}} V}{F^{\mathrm{t}}_{\mathrm{tot_o}}} \tag{24}$$

$$\mathrm{Tu} = \frac{A U_{\mathrm{H_2}} (P^{\mathrm{t}}_{\mathrm{tot}})^{1/2}}{F^{\mathrm{t}}_{\mathrm{tot_o}}} = \frac{A \rho_{\mathrm{MA}} (P^{\mathrm{t}}_{\mathrm{tot}})^{1/2}}{\delta F^{\mathrm{t}}_{\mathrm{tot_o}}} \tag{25}$$

The tube Damkohler, Da^{t}, number increases with temperature, residence time and the H_2S composition but decreases along the reactor length and eventually gets to zero if the reaction reaches equilibrium. However, by transferring the hydrogen product through the membrane the Da^{t} would increase with the reactor length, z. The Damkohler number at the tube inlet, $Da^{\mathrm{t}}_{\mathrm{o}}$, is defined as:

$$Da^{\mathrm{t}}_{\mathrm{o}} = \frac{-\gamma_{\mathrm{H_2S_o}} V}{F^{\mathrm{t}}_{\mathrm{tot_o}}} \tag{26}$$

Thus, Da^{t} can be expressed as a function of Da^{t}_{o}, namely;

$$Da^{\mathrm{t}} = Da^{\mathrm{t}}_{\mathrm{o}} \frac{-\gamma_{\mathrm{H_2S}}}{(-\gamma_{\mathrm{H_2S}})_{\mathrm{o}}} \tag{27}$$

The dimensionless number, Tu, which was first introduced by Itoh et al. [21], represents the ratio of the hydrogen permeation rate to the feed rate. It depends on the permeability (ρ_{MA}), membrane thickness (δ) and the molar feed rate to tube ($F^{\mathrm{t}}_{\mathrm{tot_o}}$). In particular, the inlet value, $\mathrm{Tu_o}$, is given as:

$$\mathrm{Tu_o} = \frac{A \rho_{\mathrm{MA_o}} (P^{\mathrm{t}}_{\mathrm{tot}})^{1/2}}{\delta F^{\mathrm{t}}_{\mathrm{tot_o}}} \tag{28}$$

Hence, Tu can be expressed as function of $\mathrm{Tu_o}$:

$$\mathrm{Tu} = \mathrm{Tu_o} \frac{\rho_{\mathrm{MA}}}{\rho_{\mathrm{MA_o}}} \tag{29}$$

The pressure ratio, R_p, in Eqs. (21b) and (21d) represents the ratio of the total pressure between the shell and the tube sides and is given as:

$$R_p = \frac{P^s_{tot}}{P^t_{tot}} \tag{30}$$

while the parameter, R_f, is given by:

$$R_f = \frac{F^t_{tot_o}}{F^s_{tot_o}} \tag{31}$$

J_{H_2} represents the dimensionless flux of H_2 through the membrane:

$$J_{H_2} = Tu_{H_2}((y^t_{H_2})^{1/2} - (R_p y^s_{H_2})^{1/2}) \tag{32}$$

Eq. (32) is the dimensionless version of Eqs. (7) or (10). NHR is the dimensionless heat of reaction:

$$NHR = \frac{-\Delta H_{rxn}}{T^t_o C_{p^t_{mix_o}}} \tag{33}$$

The Stanton number for the tube- and shell-sides are further given by:

$$St^t = \frac{U^{tg}\pi D_t L}{F^t_{tot_o} C_{p^t_{mix_o}}} = St^t_o \left(\frac{U^{tg}}{U^{tg}_o}\right) \tag{34}$$

$$St^s = \frac{h^f \pi D_s L}{F^s_{tot_o} C_{p^s_{mix_o}}} = St^s_o \left(\frac{h^f}{h^f_o}\right) \tag{35}$$

$$St^t_s = \frac{U^{tg}\pi D_t L}{F^s_{tot_o} C_{p^s_{mx_0}}} = St^t_{s_o} \left(\frac{U^{tg}}{U^{tg}_o}\right) \tag{36}$$

where St^t_o, St^s_o and $St^t_{s_o}$ are the Stanton numbers calculated at the inlet conditions. U^{tg}, which is the overall heat transfer coefficient is defined as:

$$U^{tg} = \left[\frac{1}{h_{io}} + \frac{1}{h_o}\right]^{-1} \tag{37}$$

For simplicity, the heat transfer coefficients are assumed to be constant over the reactor length. Hence, the ratio (U^{tg}/U^{tg}_o) and (h^f/h^f_o) are both unity. Finally, the wall temperature T_w, which is needed to calculate the permeability of the metal may be obtained from:

$$T_w = \frac{T^s + R_h T^t}{1 + R_h} \tag{38}$$

where R_h is the ratio of the heat transfer coefficients, h_{io}/h_i as specified in the nomenclature.

3. Results and discussions

The system of ordinary differential equations (Eqs. (21a–f)) can be solved as an initial-value problem using a fourth order Runge-Kutta method. The initial molar compositions, total molar flow rates $F^t_{tot_o}$ and $F^s_{tot_o}$; temperatures T^t_o, T^s_o, T_f and pressures P^t_{tot} and P^s_{tot} must be known. These data and the reactor characteristics are provided in Table 1 and used to calculate the required parameters in Eqs. (21a–f).

The Runge-Kutta integration is a straightforward exercise for the co-current case where the inlet to the tube and shell sides are at the same end of the double-pipe reactor assembly since it can be treated as an initial-value problem. However, the counter-current case is a nonlinear boundary-value problem since the tube inlet (whose initial conditions are known) is at the same end as the shell-side exiting stream (with unknown final conditions). A shooting method rather than finite difference approach was employed due to the nonlinear character of the governing ODEs. Thus, in the counter-current situation, the gas composition profiles within the shell-side (annulus) were initially assumed to be constant in order to solve for the tube-side composition profiles. Subsequently, the shell-side ODEs were then solved using the most recently obtained tube-side composition data. This procedure was repeatedly looped until the percentage variation in the shell-side outlet conditions for successive iterations was less than 1×10^{-2}. The CPU time to run simulations for both Runge-Kutta and Shooting methods was about 50 s and 10 min respectively on a Pentium IV 2GB Ram machine.

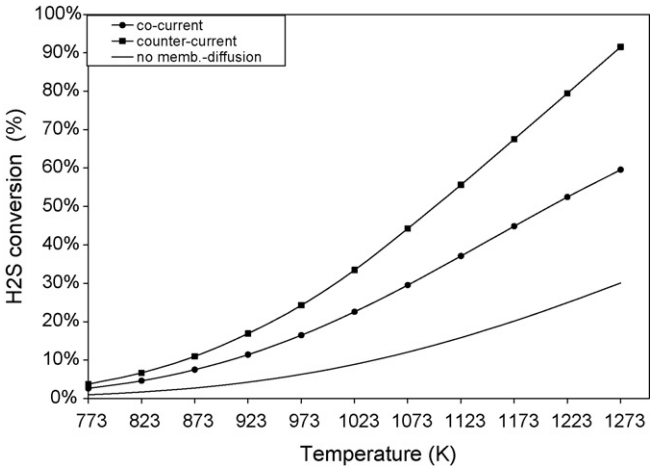

Fig. 5. Effect of temperature on H_2S conversion at rtt = 600 s, rts = 600 s, R_p = 1.

The results of the modeling are shown in Figs. 5–11. The tube feed composition was 20% H_2S/argon for all the runs. The sweep gas was taken as pure argon. The fluid residence time for the tube (rtt) and shell (rts) sides were based on the feed molar flow rate through the catalyst bed and annular volume respectively:

$$rtt = \frac{V\rho^t_{mol}}{F^t_{tot}} \tag{39}$$

$$rts = \frac{V^s\rho^s_{mol}}{F^s_{tot}} \tag{40}$$

The temperatures of the furnace, tube and shell inlets were assumed to be equal. Thus, only the inlet temperature is specified. The reactor was operated at 101.3 kPa and the changes in shell-side

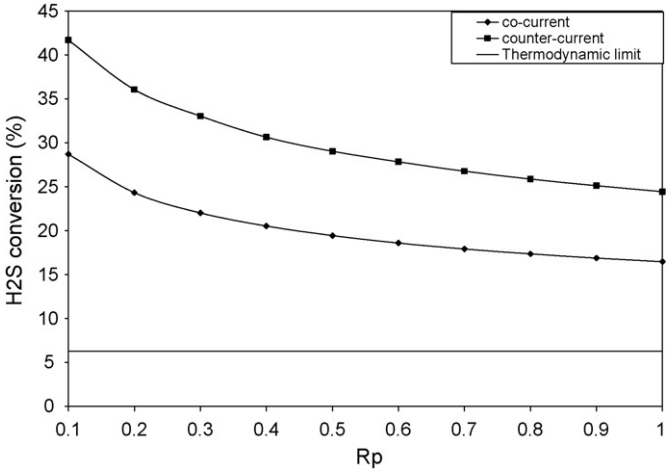

Fig. 6. Effect of shell-tube side pressure ratio on H_2S conversion at $T^t_o = 973$ K, rtt = 600 s, rts = 600 s ($Da^t_o = 319$, $Tu_o = 3.8$).

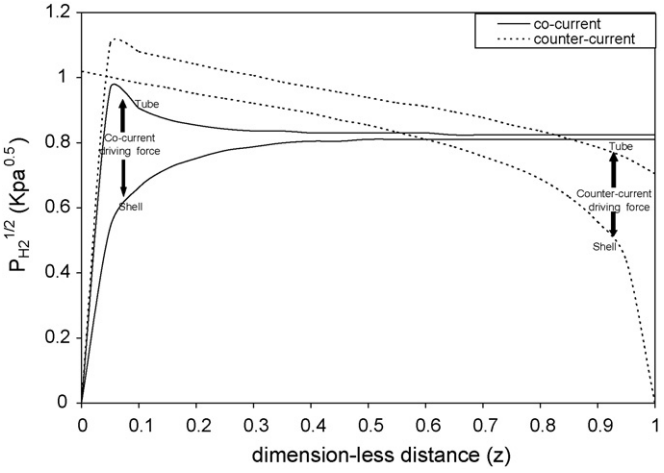

Fig. 7. Hydrogen mass transfer driving force ($P_{H_2}^{t\ 1/2} - P_{H_2}^{s\ 1/2}$) along the reactor for the co- and counter-current operations ($T_o^t = 973$ K, rtt = 600 s, rts = 600 s, $R_p = 0.9$, $Da_o^t = 319$, $Tu_o = 3.8$).

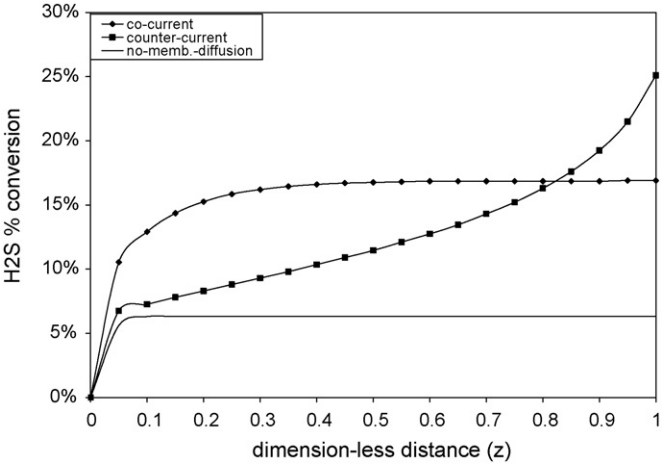

Fig. 8. H_2S conversion along the reactor for the co and counter-current arrangement ($T_o^t = 973$ K, rtt = 600 s, rts = 600 s, $R_p = 0.9$, $Da_o^t = 319$, $Tu_o = 3.8$).

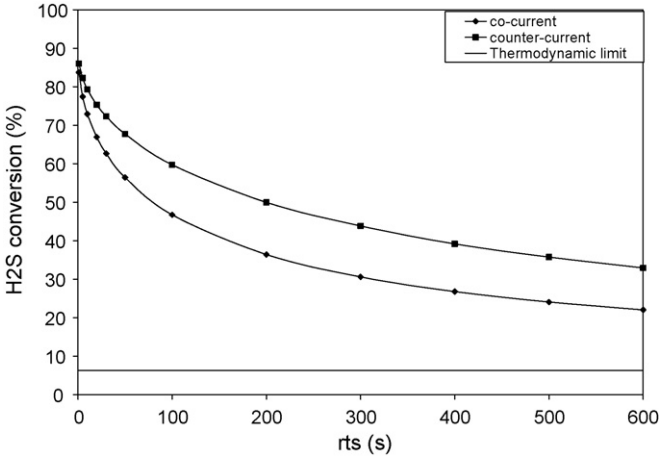

Fig. 9. Effect of the shell residence time (rts) on H_2S conversion at $T_o^t = 973$ K, rtt = 600 s, $R_p = 0.3$ ($Da_o^t = 319$, $Tu_o = 3.8$).

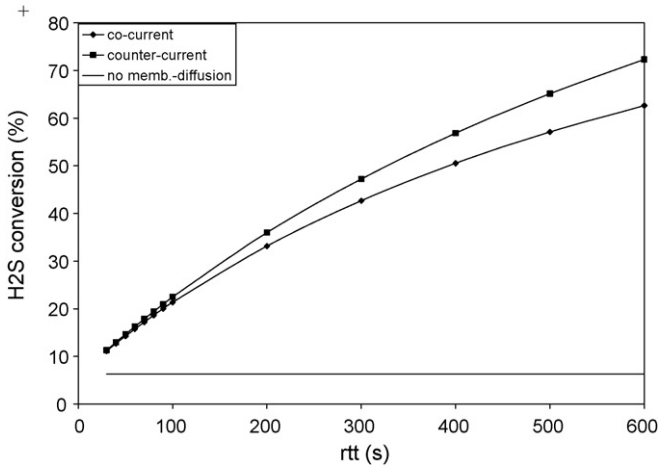

Fig. 10. Effect of the tube residence time (rtt) on H_2S conversion at $T_o^t = 973$ K, rts = 30 s, $R_p = 0.3$.

pressure are reported via the dimensionless number, R_p. The membrane reactor characteristics were kept constant (cf. Table 1) in all simulations except in Fig. 11 where the effect of the thickness of the Pt coating was a variable.

Fig. 5 shows the effect of inlet temperature on the H_2S conversion. It is seen that the conversion increases with temperature, which is consistent with the endothermic nature of the reversible reaction. Significantly, the conversion in the double-pipe catalytic packed bed membrane reactor is superior to the operation with a non-permeable tube wall. Additionally, the counter-current reactor offers a better performance at all temperatures than the co-current operation. This is consistent with a shift to the right in the reaction equation (cf. Eq. (14)) as predicted by Le Chatelier's principle, as H_2 simultaneously diffuses through the membrane walls during H_2S decomposition. As expected, the conversion in all three cases exhibit Arrhenius-dependency on temperature.

Fig. 6 reveals that the reduction in shell-side pressure drop relative to the tube-side (decreasing R_p) increases H_2S conversion possibly due to higher transmembrane pressure gradient. The superiority of the counter-current operation to the co-current mode is also evident from these data. Indeed, the parallel nature of the two conversion profiles over the range of R_p examined indicates that similar hydrogen transport mechanisms governed the

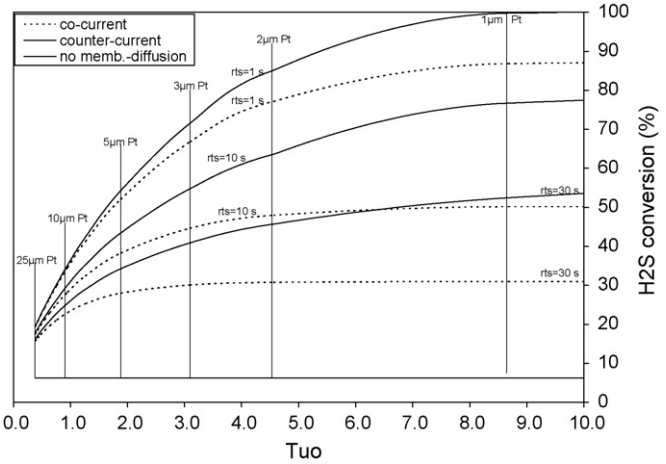

Fig. 11. Effect of the Tu_o number on H_2S conversion at $T_o^t = 973$ K, rtt = 60 s, $R_p = 0.3$ at three rts levels: 1, 10 and 30 s.

behaviour during both forms of operation. Significantly, conversion under membrane operation was 3–7 times higher than the thermodynamic estimate. More importantly, the use of low sweep gas pressure would reduce operating costs and favour subsequent separation of H_2 from inert Ar.

Fig. 7 plots the transmembrane driving force, $(P_{H_2}^{t\ 1/2} - P_{H_2}^{s\ 1/2})$ as a function of the reactor length. For the co-current reactor, the H_2 partial pressure in the tube-side (packed bed) goes through an initial overshoot near the reactor entrance ($z < 0.1$) before relaxing to a constant level at $z > 0.4$. The appearance of an overshoot (or undershoot) in composition (or conversion) profiles in fixed bed catalytic reactors has precedence in the literature especially in the case of non-isothermal reversible reactions such as NH_3 synthesis and SO_2 oxidation [22]. The phenomenon is due to the interaction between the reversible form of the kinetic expression (with non-linear Arrhenius-dependency on temperature in both forward and backward rate constants) and the magnitude of reaction thermicity. For example, the governing reversible rate expressions for catalytic NH_3 synthesis and SO_2 oxidation are similar to the situation in H_2S decomposition (cf. Eq. (15)). This lends credence to the attribution of the overshoot in the composition profile to nonlinearity in the rate expression. The H_2 profile within the shell-side, however, rises rapidly to a plateau just marginally below the H_2 pressure in the tube-side, within the same distance ($0 < z < 0.4$). This is consistent with the negligible reaction taking place in the shell-side. It is apparent from this behaviour that the driving force across the membrane is practically nil after about 40% of the reactor length. Indeed, the transmembrane pressure drop is higher at dimensionless distance less than 0.4 but continuously decreases along the reactor length reaching a plateau close to the outlet. Thus, in the last half of the reactor the low hydrogen transfer rate kept the H_2S conversion almost constant. This is confirmed by the axial H_2S conversion profile shown in Fig. 8.

Interestingly, in the counter-current operation, although hydrogen production exhibits a similar overshoot (cf. Fig. 7), it displays a larger negative axial pressure gradient over the entire reactor length with a concomitant positive axial H_2 pressure gradient in the shell-side. The existence of an overshoot in the axial H_2 concentration profile in spite of this direction change further reinforces causative role of nonlinear interaction as being rooted in the structural form of the reversible rate law. It is evident that the type of axial composition profile in a catalytic packed bed reactor is intricately linked to the nature of the reaction mechanism.

Nevertheless, since the permeation coefficient is the same for both co-current and counter-current flows, it is apparent that the counter-current operation is a more effective gas separation mode. In the counter-current arrangement, the transmembrane driving force is smaller than in the co-current one at the beginning of the reactor. In fact, near the reactor inlet (shell exit) a negative H_2 transfer is possible (from shell-to-tube side) probably due to the low H_2S conversion near the inlet and a correspondingly higher H_2 content in the sweep gas. However, contrary to the co-current arrangement, the driving force increases along the reactor becoming higher during the second half of the tube. As a result, there is an important hydrogen transfer toward the end of the reactor shifting the equilibrium to the right and hence, an increased H_2S conversion as evident in Fig. 8.

Fig. 9 shows the effect of shell-side residence time (rts) on the H_2S conversion. It is seen that reduction in rts increased H_2S conversion. Clearly, increasing sweep gas flow rate increases the H_2 flux through membrane by keeping the shell hydrogen concentration profile low. The figure also shows that conversions during membrane operation are well above (>3) the theoretical equilibrium limit. However, in practice the recovery of H_2 from such large argon flow rates (in downstream reactor sections of the plant) may be a constraint on the choice of rts employed for the membrane reactor.

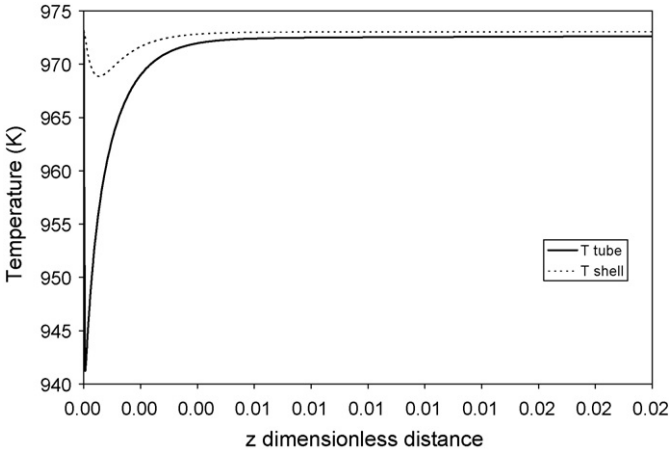

Fig. 12. Temperature profile at the inlet in the co-current operation at $T_o^t = 973$ K, $T_o^t = 973$ K, rtt = 600 s, rts = 600 s ($Da_o^t = 319$, $Tu_o = 3.8$, $R_p = 0.9$).

The effect of reducing the tube-side residence time (rtt) on the conversion is shown in Fig. 10. As expected, H_2S conversion is reduced by decreasing the rtt due to the reduction in the Damkohler number, Da^t. For instance, the H_2S conversion is reduced from 62.2% to 15.7% by changing the rtt from 600 to 60 s in the co-current arrangement, and from 72.3% to 16.2% on the counter-current one. It is also apparent that the counter-current operation gave higher H_2S conversions in the range of rtt examined.

Additional improvements in the conversion may be obtained by increasing the hydrogen membrane permeability ρ_{MA}. Fig. 11 shows the conversion as a function of the Tu_o number. The major resistance to mass transfer through the membrane is caused by the Pt thickness that has a permeability of about four orders of magnitude lower than Nb. Thus, the Tu_o number can be increased by reducing the thickness of the platinum coating. The plot shows that high conversions can be achieved with small shell residence times by reducing the thickness of the platinum layer. In practice, extremely thin Pt coating may be unreliable for extended use due to development of hairline cracks at high reaction temperatures. Even so, Kikuchi [23] has reported that Pt coating as low as 2 μm may be conveniently obtained by CVD and is structurally stable up to 1200 K.

Fig. 12 displays the temperature profile of the co-current operation. It shows that the tube temperature dropped sharply from the inlet temperature, 973–943 K just after the reactor inlet ($0 < z < 0.0002$) thereafter it rose monotonically to almost thermal equilibrium with the shell-side at $z > 0.020$. This highly steep undershoot in temperature is a reflection of the large endothermic heat of reaction which occasioned an abrupt drop in temperature almost immediately after entering the reactor tube. This is consistent with the overshoot in H_2 production (over the same axial distance). The flow-on effect of the large drop in tube-side temperature is also evident in the shell-side temperature, albeit with a much more attenuated drop (about 5 K compared to 30 K in the tube-side).

4. Conclusions

A detailed analysis of hydrogen production from H_2S decomposition in a catalytic packed bed double-pipe membrane reactor has demonstrated that it is possible to exceed the thermodynamic ceiling by two- to five-fold-improvement for this equilibrium constrained endothermic reaction. The modeling showed that oper-

ation in the counter-current mode gave better H_2 yield than in the co-current strategy. Although the Nb membrane inner tube has to be coated with Pt to improve the resistance against H_2S attack, our analysis demonstrated that an optimum Pt thickness of about 1 μm is required to achieve nearly complete H_2S conversion. The model was also made more realistic than previous membrane reactor treatments by the inclusion of a criterion that admitted the temperature-dependency of membrane permeability. The findings of this study showed that the practical implementation of a shell and tube catalytic packed membrane reactor is possible and indeed, independent experimental results in our laboratory have provided supportive evidence with up to 300% increase in H_2 yield seen under some conditions [24].

Acknowledgments

The authors are grateful to the Australian Research Council for financial support.

References

[1] E.A. Fletcher, J.E. Noring, J.P. Murray, Hydrogen sulfide as a source of hydrogen, Int. J. Hydrogen Energy 9 (1984) 587–593.
[2] D. Kirk-Othmer, Encyclopedia Chemical Technology, John Wiley & Sons, New York, 1984.
[3] M.E.D. Raymont, Make hydrogen from hydrogen sulfide, Hydrocarbon Process. 54 (1975) 139–142.
[4] V. Kaloidas, N. Papayannakos, Kinetics of thermal, non-catalytic decomposition of hydrogen sulphide, Chem. Eng. Sci. 44 (1989) 2493–2500.
[5] A.A. Adesina, V. Meeyoo, G. Foulds, Thermolysis of hydrogen sulphide in an open tubular reactor, Int. J. Hydrogen Energy 20 (1995) 777–783.
[6] K.A. Hawboldt, W.D. Monnery, W.Y. Svrcek, New experimental data and kinetic rate expression for H_2S pyrolysis and re-association, Chem. Eng. Sci. 55 (2000) 957–966.
[7] H. Ohashi, H. Ohya, M. Aihara, Y. Negishi, S.I. Semenova, Hydrogen production from hydrogen sulfide using membrane reactor integrated with porous membrane having thermal and corrosion resistance, J. Membr. Sci. 146 (1998) 39–52.
[8] P.P.Y. Chan, K. Vanidjee, A.A. Adesina, P.L. Rogers, Modeling and simulation of non-isothermal catalytic packed bed membrane reactor for H_2S decomposition, Catal. Today 63 (2000) 379–385.
[9] H. Ohashi, H. Ohya, M. Aihara, T. Takeuchi, Y. Negishi, J. Fan, S.I. Semenova, Analysis of a two-stage membrane reactor integrated with porous membrane having Knudsen diffusion characteristics for the thermal decomposition of hydrogen sulfide, J. Membr. Sci. 166 (2000) 239–247.
[10] R. Govind, D. Atnoor, Development of a composite palladium membrane for selective hydrogen separation at high temperature, Ind. Eng. Chem. Res. 30 (1991) 591–594.
[11] N. Itoh, A membrane reactor using palladium, AIChE J. 33 (1987) 1576–1579.
[12] N. Itoh, W.-C. Xu, K. Haraya, Basic experimental study on palladium membrane reactors, J. Membr. Sci. 66 (1992) 149–155.
[13] D.J. Edlund, W.A. Pledger, Thermolysis of hydrogen sulfide in a metal-membrane reactor, J. Membr. Sci. 77 (1993) 255–264.
[14] R.E. Buxbaum, A.B. Kinney, Hydrogen transport through tubular membranes of palladium-coated tantalum and niobium, Ind. Eng. Chem. Res. 35 (1996) 530–537.
[15] K. Fukuda, M. Dokiya, Y. Kotera, Catalytic decomposition of hydrogen sulfide, Ind. Eng. Chem. Fundam. 17 (1978) 243–248.
[16] V.E. Kaloidas, N.G. Papayannakos, Kinetic studies on the catalytic decomposition of hydrogen sulfide in a tubular reactor, Ind. Eng. Chem. Res. 30 (1991) 345–351.
[17] M. Gwaunza, A.A. Adesina, The performance of a Ru-Mo sulfide catalyst for H_2S decomposition, React. Kinet. Catal. Lett. 62 (1997) 55–62.
[18] S.C. Moffat, A.A. Adesina, The dissociation kinetics of H_2S over an alumina supported Co-Mo sulphide catalyst, Catal. Lett. 37 (1996) 167–172.
[19] J. Zaman, A. Chakma, A simulation study on the thermal decomposition of hydrogen sulfide in a membrane reactor, Int. J. Hydrogen Energy 20 (1995) 21–28.
[20] M.K. Koukou, G. Chaloulou, N. Papayannakos, N.C. Markatos, Mathematical modelling of the performance of non-isothermal membrane reactors, Int. J. Heat. Mass Transfer 40 (1997) 2407–2417.
[21] N. Itoh, Y. Shindo, K. Haraka, Ideal flow models for palladium membrane reactors, J. Chem. Eng. Jpn. 23 (1990) 420–425.
[22] H.S. Fogler, Elements of Chemical Reaction Engineering, third ed., Prentice-Hall, Englewood Cliffs, NJ, 1999.
[23] E. Kikuchi, Hydrogen permselective membrane reactor, CATTECH (1997) 67–74.
[24] P.P.Y. Chan, PhD thesis, School of Chemical Sciences and Engineering, University of New South Wales, Sydney, 2006.